Molecular BioSystems

Dynamic Article Links

Cite this: *Mol. BioSyst.*, 2011, **7**, 3343–3352

www.rsc.org/molecularbiosystems

PAPER

Fluorescent labeling agents change binding profiles of glycan-binding proteins†

Yiyan Fei,[a] Yung-Shin Sun,[a] Yanhong Li,[b] Kam Lau,[b] Hai Yu,[b] Harshal A. Chokhawala,[b] Shengshu Huang,[b] James P. Landry,[a] Xi Chen[b] and Xiangdong Zhu*[a]

Received 10th August 2011, Accepted 20th September 2011
DOI: 10.1039/c1mb05332a

Interactions of glycan-binding proteins (GBPs) with glycans are essential in cell adhesion, bacterial/viral infection, and cellular signaling pathways. Experimental characterization of these interactions based on glycan microarrays typically involves (1) labeling GBPs directly with fluorescent reagents before incubation with the microarrays, or (2) labeling GBPs with biotin before the incubation and detecting the captured GBPs after the incubation using fluorescently labeled streptavidin, or (3) detecting the captured GBPs after the incubation using fluorescently labeled antibodies raised against the GBPs. The fluorescent signal is mostly measured *ex situ* after excess fluorescent materials are washed off. In this study, by using a label-free optical scanner for glycan microarray detection, we measured binding curves of 7 plant lectins to 24 glycans: four β1-4-linked galactosides, three β1-3-linked galactosides, one β-linked galactoside, one α-linked *N*-acetylgalactosaminide, eight α2-3-linked sialosides, and seven α2-6-linked sialosides. From association and dissociation constants deduced by global-fitting the binding curves, we found that (1) labeling lectins directly with fluorescent agents change binding profiles of lectins, in some cases by orders of magnitude; (2) those lectin–glycan binding reactions characterized with large dissociation rates, though biologically relevant, are easily missed or deemed insignificant in *ex situ* fluorescence-based assays as most captured lectins are washed off before detection. This study highlights the importance of label-free real-time detection of protein–ligand interactions and the potential pitfall in interpreting fluorescence-based assays for characterization of protein–glycan interactions.

Introduction

Protein interactions with carbohydrates presented on host cellular surfaces are essential in cell adhesion, bacterium/virus-host interaction, and cellular signaling in living systems.[1–4] System-wide studies of protein–glycan interaction have followed the heels of genomic and proteomic research. The role of glycans in cellular processes is complex and at same time promising for drug development and health improvement. The complexity is due in part to the structure diversity of glycans in comparison with those of DNA and protein molecules (even considering that the latter are further organized into higher-order structural forms), and partly due to less research that has so far been directed to glycobiology. The recent emergence of glycan microarrays and high-throughput synthesis of glycans presents promising platforms for characterization of protein–glycan, virus-glycan, and bacterium-glycan interactions, and in turn to accelerate the pace of glycomic studies.[5–12]

Binding profiles of glycan-binding proteins (GBP) are useful for identifying reagents with high specificities for tissue or cell staining to unveil spatial distributions of different glycan types. For example, *Maackia amurensis* Lectin (MAA) highlights the presence of α2-3-linked sialosides while *Sambucus nigra* Lectin (SNA) maps out the distribution of α2-6-linked sialosides.[13] Wheat germ agglutinin (WGA) reports densities of GlcNAc and Galβ1-4GlcNAc. Hemagglutinins (HAs) from seasonal human influenza A viruses prefer to bind α2-6-linked sialosides, while HAs from seasonal avian influenza A viruses favor α2-3-linked sialosides.[9] Furthermore, binding profiles of glycan-binding

[a] *Department of Physics, University of California at Davis, Davis, California 95616, USA. E-mail: xdzhu@physics.ucdavis.edu; Fax: +1 530-752-4717; Tel: +1 530-752-4689*
[b] *Department of Chemistry, University of California at Davis, Davis, California 95616, USA*

† Electronic supplementary information (ESI) available: Drawings of 24 oligosaccharides used in this study are depicted in Fig. S1. Binding profiles of ECA, PNA, MAA, WFA, and SNA with and without FITC labeling are listed as Fig. S2 through Fig. S6. Tables of equilibrium dissociation constants of 7 non-labeled and FITC-labeled lectins with 24 glycans are tabulated in Table S1 through Table S8. See DOI: 10.1039/c1mb05332a

proteins on the membrane surface of a bacterial or a viral particle can be used to distinguish different bacterial or viral strains.[9]

Experimental measurements of binding profiles of GBPs on glycan microarrays are mostly fluorescence-based.[5–12] These involve labeling GBPs with fluorescent agents either directly, or indirectly by conjugating the GBPs with biotin or Fc fragments of human IgG or precomplexing the GBPs with anti-GBP antibodies before incubation with glycans and then followed by reactions with fluorescent-labeled streptavidin or secondary antibodies.[4,8,9,12] The unbounded proteins and protein complexes are washed off thoroughly before endpoints of the GBP-glycan reactions are detected with a fluorescence scanner. There are two general problems with such ex-situ fluorescence-based detection. Post-reaction washing removes most captured GBPs with equilibrium dissociation constants K_D in the range of μM to *sub*-mM. Even for captured GBPs that survive washing, their binding profiles are subject to change due to conjugation with fluorescent agents or pre-complex formation with antibodies before reaction with glycans. Often the effect of direct fluorescent labeling or conjugation with Fc fragment of human IgG or precomplex formation with anti-GBP antibodies on the binding profile of a GBP is not fully characterized, if at all.[9] Consequently experimental binding profiles deduced from fluorescence measurements can be significantly inaccurate, and thus subsequent applications of these profiles to glycan distribution mapping should be taken with caution to avoid erroneous interpretation.

We report a direct experimental study of the effect of fluorescent labeling on binding profiles of glycan-binding proteins (GBPs). We measured equilibrium association constants of 7 plant lectins, with and without fluorescein isothiocyanate (FITC) conjugated to the lysine residues or the terminal amino groups of the proteins, to 24 glycans in a glycan microarray immobilized on a streptavidin functionalized glass surface. The glycans include 15 sialosides, eight α2-3-linked and seven α2-6-linked. The equilibrium association constants are extracted from the binding curves to the glycans detected using an ellipsometry-based optical scanning microscope.

Results

Fluorescence-labeling of lectins alters the binding curves of the lectins to glycan targets

Fig. 1 shows the association–dissociation curves (binding curves) of FITC-labeled and non-labeled WGA and MAA to 24 oligosaccharides as listed in Table 1 (the drawings of these oligosaccharides can be found in Supplementary Information). The solid lines are global fits to a two-site Langmuir reaction model that will be described below. It is immediately clear that the binding profiles of these two plant lectins (glycan-binding proteins) are profoundly changed by FITC labeling. Non-labeled WGA binds to both α2-3-(OS-10 through OS-17) and α2-6-linked (OS-18 and OS-21 through OS-24) sialosides, while FITC-labeled WGA only binds to α2-3-linked sialosides. FITC labeling also reduces the affinity of MAA to four α2-3-linked sialosides (OS-11 through OS-14) (see Supplementary Information for details). Non-labeled MAA binds to Galβ1-4GlcNAc**6S**β (OS-6), while FITC-MAA binds to Galβ1-4GlcNAcβ (OS-5) instead.

Endpoint assays of lectin–glycan reactions depend on how reactions end

Another clearly noticeable feature is that dissociation times of FITC-MAA from four α2-3-linked sialosides (OS-11 through OS-14), Neu5Acα2-3Galβ1-4Glcβ-, Neu5Acα2-3Gal6Sβ1-4Glcβ-, Neu5Acα2-3Galβ1-4GlcNAcβ-, Neu5Acα2-3Galβ1-4GlcNAc6Sβ-, are dramatically shortened so that an endpoint assay of these binding reactions after the lectin solution is removed easily misses the evidence of the reaction. This is best illustrated in Fig. 2 which shows the change in surface mass density of the glycan microarray before and after incubation with non-labeled and FITC-labeled MAA. While the evidence of non-labeled MAA binding reactions with four sialosides remains strong, the evidence is essentially missing for FITC-labeled MAA reactions with the four sialosides due to much faster dissociation rates.

Lectin reactions with immobilized glycan targets are described by two-site Langmuir reaction model

The third prominent feature revealed in Fig. 1 is that most binding curves cannot be fitted to a 1-to-1 Langmuir reaction model,[14] unlike association–dissociation curves of monoclonal antibodies to surface-bound antigens. The goodness-of-fit is based on how close the ratio of the fitting residual to the standard variation of the data is to unity. For all the lectins investigated in this work, the two-site model consistently yields a better fit than does the one-site model. This may not be surprising for two reasons: (i) lectins can have more than one binding pocket for glycan receptors; and (ii) a surface-bound glycan can present itself in more than one stereochemical configuration. For fluorescently labeled lectins, they are often inhomogeneous mixtures with an average number of fluorophores per lectin molecule as supplied by the vendors (see Materials and Methods Section). This makes differently labeled lectins another contributing factor to the need of the two-site model. Since sizes of the plant lectins used in this study are comparable to or larger than the size of streptavidin tetramers (52 kDa) used to immobilize biotin-conjugated oligosaccharides on a glass surface (see Materials and Methods section), each lectin has access to more than one immobilized oligosaccharide (if energetically favorable) so that the lectin binding can enter into a "multi-valence" configuration with multiple glycan targets dominated by one of them. To extract key characteristics of lectin–glycan binding reactions with the fewest number of fitting parameters, we find it necessary and sufficient to use a two-site Langmuir reaction model.[14] In this model, a lectin is assumed to bind to surface-bound glycans in two possible configurations (or loosely "sites" of binding), each with a distinct association rate constant (k_{on}), a dissociation rate constant (k_{off}) and in turn an equilibrium association constant $K_a = k_{on}/k_{off} = 1/K_d$ (K_d is the dissociation constant).

The binding curves of a lectin to glycan targets in three lectin concentrations were globally fitted to the two-site Langmuir reaction model, with association and dissociation rate constants and relative coverage of each "site" as fitting parameters. The fits are shown in solid lines in Fig. 1 for WGA and MAA. From the association and dissociation rate constants, we compute equilibrium association constants $K_a = k_{on}/k_{off}$ and use K_a to represent affinity constants.

The affinity constant profiles for WGA and RCA, with and without FITC labeling, are shown in Fig. 3 and 4. The affinity profiles for the remaining 5 lectins, along with Tables of equilibrium dissociation constants $K_d = 1/K_a = k_{off}/k_{on}$ are listed in Supplementary Information.

WGA-glycan binding profile

The affinity constant profile is changed dramatically by FITC-labeling (Fig. 3). Non-labeled WGA binds to GalNAcα (OS-2) and Galβ1-4GlcNAcβ (OS-5) and Galβ1-4GlcNAc6Sβ (OS-6) with K_a around 1 nM^{-1} (or $K_d \sim 1$ nM). All 8 α2-3-linked sialosides and 5 out of 7 α2-6-linked sialosides have K_a around 0.01 nM^{-1} (or $K_d \sim 100$ nM).[15–18] Most noticeable observation is that FITC-WGA no longer binds to Neu5Acα2-6Galβ in our present label-free binding assay which has a detection limit of $K_d \sim 500$ μM. Labeling WGA with FITC decreases the binding affinity of WGA to GalNAcα and Galβ1-4GlcNAc(**6S**)β by as much as 5 orders of magnitude. Though it is generally expected that fluorescent labels are prone to alter the binding property of a glycan-binding protein, we are not aware of other label-free studies in the literature that directly examine how binding affinity constants of glycan-binding

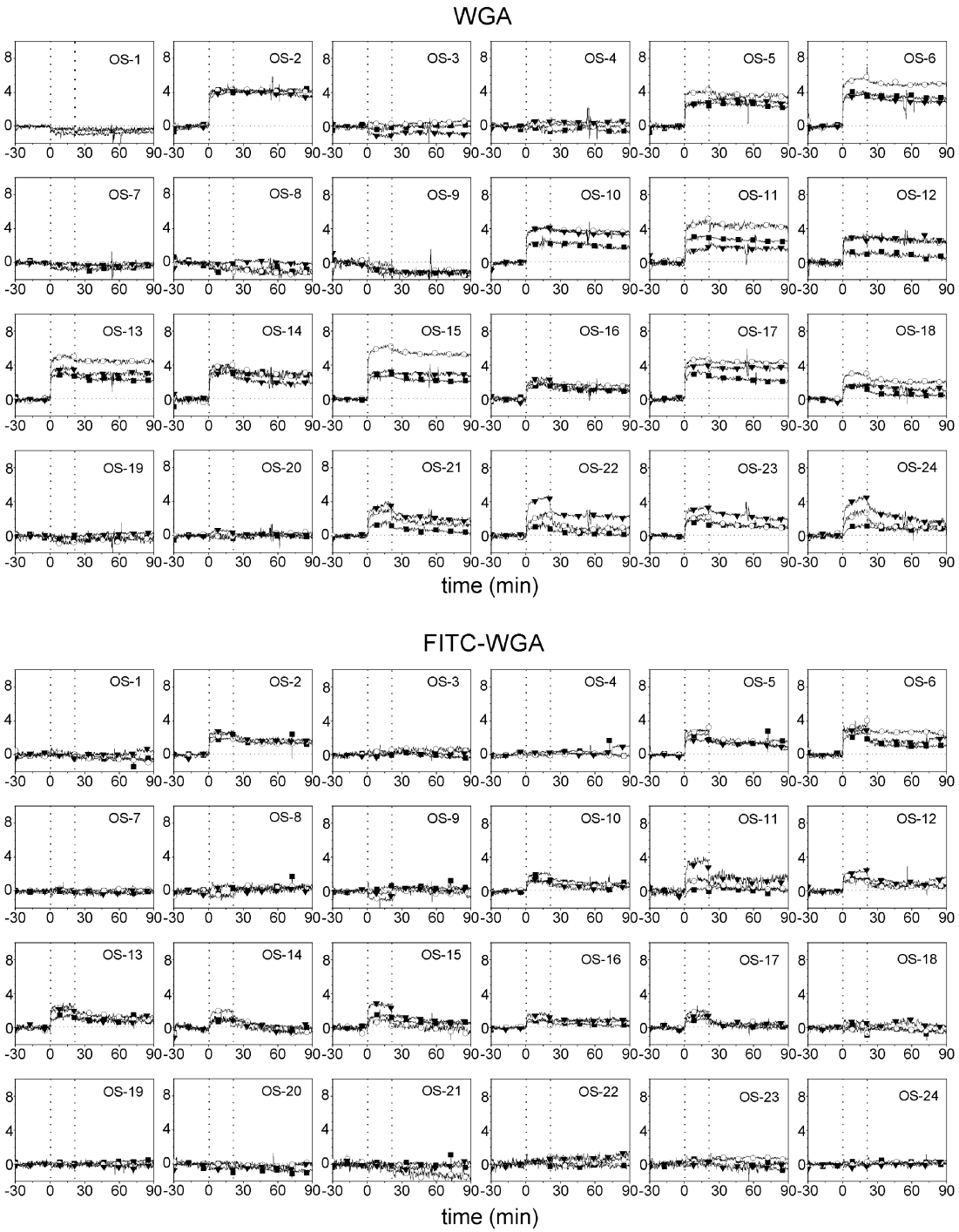

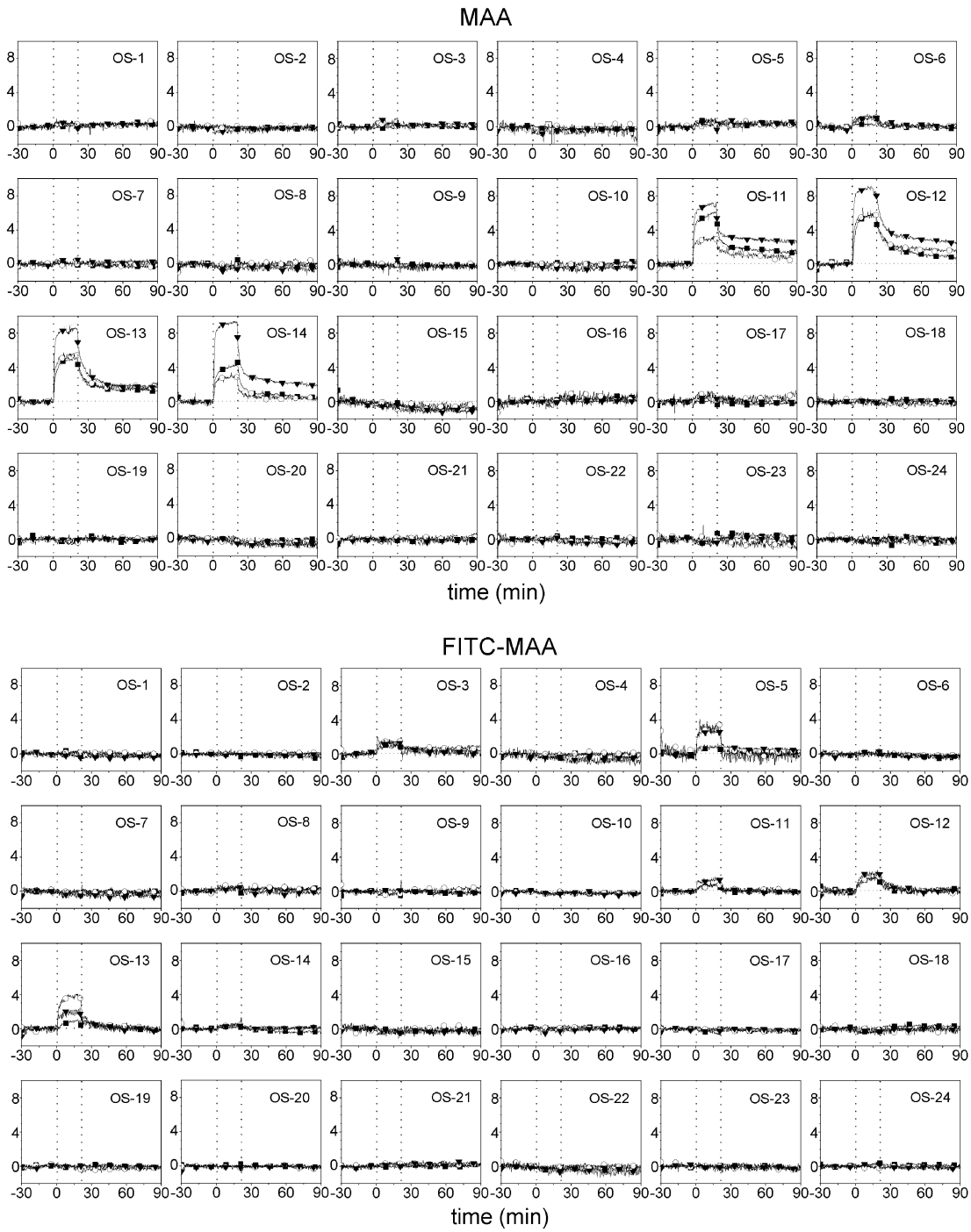

Fig. 1 Association–dissociation curves of WGA and MAA binding to 24 oligosaccharides. One unit of the optical signal corresponds to a protein surface mass density of 5×10^{-8} g cm^{-2}, assuming that the protein volume mass density is 1.35 g cm^{-3}. (a) Non-labeled WGA in 1×PBS at a concentration of 5.7 μM (solid squares), 11.4 μM (open circles), and 22.7 μM (solid triangles); (b) FITC-WGA in 1×PBS at a concentration of 5.7 μM, 11.4 μM, and 22.7 μM; (c) non-labeled MAA in 1×PBS at a concentration of 0.75 μM (solid squares), 1.5 μM (open circles), and 3 μM (solid triangles); (d) FITC- MAA in 1×PBS at a concentration of 0.75 μM, 1.5 μM, and 3 μM. Vertical lines mark the starts of association and dissociation phases of the binding event, respectively. The solid lines through the curves are global fits to a two-site Langmuir reaction model to yield equilibrium association constants.

proteins change as a result of adding only fluorescent labels to the proteins.

RCA-glycan binding profile

The affinity profile is also changed significantly by FITC-labeling, more noticeable for some glycan targets (Fig. 4). Non-labeled RCA binds to Galβ- (OS-1), Galβ1-4Glcβ (OS-3), Gal**6S**β1-4Glcβ (OS-4), Galβ1-4GlcNAcβ (OS-5)[31] and all 7 α2-6-linked sialosides (OS-18 through OS-24)[19,20] with K_d in the range of 1 nM to 100 nM. Non-labeled lectin binds additionally to Galβ1-3GlcNAcβ (OS-7) and Galβ1-4GalNAcβ- (OS-9). Most noticeable change due to FITC labeling

Table 1 A list of 24 biotinylated oligosaccharides and assigned identification numbers used for lectin binding profile measurements in the present work

Glycan I.D.	Glycan structures				
OS-1		Gal	β-Biotin		
OS-2		GalNAc	α-Biotin		
OS-3		Gal	β1-4Glc	β-Biotin	
OS-4		Gal6S	β1-4Glc	β-Biotin	
OS-5		Gal	β1-4GlcNAc	β-Biotin	
OS-6		Gal	β1-4GlcNAc6S	β-Biotin	
OS-7		Gal	β1-3GlcNAc	β-Biotin	
OS-8		Gal	β1-3GlcNAc	β1-3Galβ1-4Glc	β-Biotin
OS-9		Gal	β1-3GalNAc	β-Biotin	
OS-10	Neu5Acα2-3	Gal	β-Biotin		
OS-11	Neu5Acα2-3	Gal	β1-4Glc	β-Biotin	
OS-12	Neu5Acα2-3	Gal6S	β1-4Glc	β-Biotin	
OS-13	Neu5Acα2-3	Gal	β1-4GlcNAc	β-Biotin	
OS-14	Neu5Acα2-3	Gal	β1-4GlcNAc6S	β-Biotin	
OS-15	Neu5Acα2-3	Gal	β1-3GlcNAc	β-Biotin	
OS-16	Neu5Acα2-3	Gal	β1-3GlcNAc	β1-3Galβ1-4Glc	β-Biotin
OS-17	Neu5Acα2-3	Gal	β1-3GalNAc	β-Biotin	
OS-18	Neu5Acα2-6	GalNAc	α-Biotin		
OS-19	Kdnα2-6	Gal	β1-4Glc	β-Biotin	
OS-20	Neu5Gcα2-6	Gal	β1-4Glc	β-Biotin	
OS-21	Neu5Acα2-6	Gal	β1-4Glc	β-Biotin	
OS-22	Neu5Acα2-6	Gal	β1-4GlcNAc	β-Biotin	
OS-23	Neu5Acα2-6	Gal	β1-4GlcNAc6S	β-Biotin	
OS-24	Neu5Acα2-6	Gal	β1-3GlcNAc	β-Biotin	

is that the labeled protein no longer binds to Gal**6S**β1-4Glcβ (OS-4), and 2 α2-6-linked sialosides Neu5Acα2-6GalNAcα (OS-18) and Neu5Acα2-6Galβ1-3GlcNAcα (OS-24). Instead, the labeled protein now binds to GalNAcα (OS-2)[14] and Galβ1-3GlcNAcβ1-3Galβ1-4Glcβ (OS-8).

Precomplexed GBPs with primary antibodies change the GBP-glycan interaction[4,8,9,12]

Since the conjugation of FITC (400 Daltons) to lectins has a profound effect on the lectin–glycan binding profile, we expect that precomplexing lectins with anti-lectin IgGs (150 kDaltons) or the Fc-fragments of IgGs (60 kDaltons) should have the similar effect, even though precomplexing lectin is one of the commonly used methods in characterizing lectin–glycan interaction. As an initial attempt to investigate the effect of precomplexing, we mixed RCA (0.67 μM) and goat anti-RCA IgG (1.34 μM) (Vector Laboratories, Burlingame, CA) and performed the binding assays on the glycan microarray under otherwise the same conditions. Fig. 5 shows the affinity constant profiles of RCA and the IgG-RCA precomplex. Precomplexing RCA with IgG substantially changed the binding profile. Notably, the IgG-RCA precomplex does not bind to Galβ1-3Glc/GalNAcβ (OS-7 and OS-9) and Neu5Acα2-6Galβ1-3GlcNAcβ (OS-24) but still binds to Galβ1-4GlcNAcβ (OS-5) and Neu5Acα2-6Galβ1-4GlcNAcβ (OS-22). Table of the equilibrium dissociation constants (Table S3) is listed in Supplementary Information.

Discussion

Accurate information on binding profiles and ligand specificities of glycan-binding proteins (GBPs) is crucial for understanding mechanisms of cellular interactions at molecular level, particularly for those related to bacterial and viral infection and cellular signaling. It is the starting point of developing effective means to enhance those interactions that are beneficial and to interrupt or deter those that disrupt normal cellular functions. Despite the routine use of fluorescence-based detection for characterizing protein–glycan interactions, the effect of such detection method on experimentally determined binding profiles is not well characterized. Our present study illustrates some key aspects of how an endpoint assay and the use of direct or indirect fluorescence labeling can lead to incomplete or in some cases grossly inaccurate binding profiles of GBPs.

Our present experimental study shows that labeling a glycan-binding protein alters the equilibrium association constant of the protein with glycan receptors by as much as orders of magnitude, and the alteration is not easily predictable for different glycans even if the latter are close analogs of each other. A case in point is that WGA binds to α2-6-linked sialosides Neu5Acα2-6Galβ (OS-18, and OS-21 through OS-24) as shown in Fig. 3 while FITC-WGA does not. As described in Materials and Methods Section, there are on average 2 FITC molecules conjugated to one WGA at its accessible primary amine sites, and 5 FITC molecules conjugated to one RCA with the same conjugation chemistry. The observed modification of glycan-binding profiles of WGA and RCA by FITC is most likely due to a steric occlusion of the glycan-binding pocket by the physical presence of FITC molecules instead of significant changes in the lectin structure in response to the conjugation. This proposition is supported by our recent finding that WGA and RCA conjugated with biotin using the same conjugation chemistry (from the same vendor) have essentially the same glycan-binding profiles as the un-conjugated (unlabeled) WGA and RCA, respectively. This means that binding profiles obtained with fluorescence-labeled GBPs can be problematic and the use of these profiles for subsequent

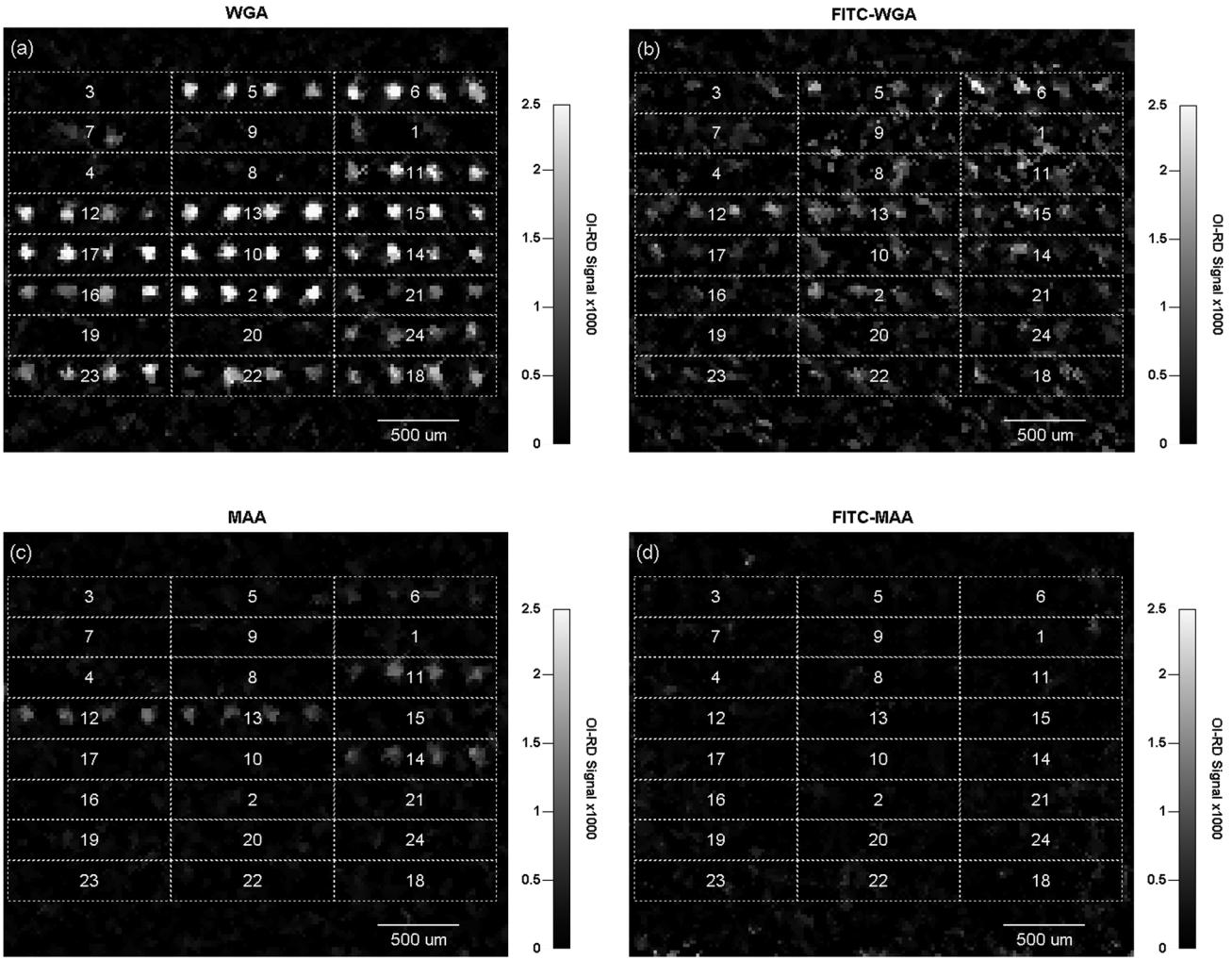

Fig. 2 Surface mass density changes on the 24-target glycan microarray after first incubation in (a) non-labeled WGA; (b) FITC-labeled WGA; (c) non-labeled MAA; (d) FITC-labeled MAA, for 30 min, and then dissociation in 1× PBS for 60 min. One unit of OI-RD signal corresponds to a protein surface mass density of 5×10^{-8} g cm^{-2}. The numbers in the panels are glycan IDs as defined in Table 1. Due to significant dissociation over 60 min, many binding events evident in binding curve measurements (Fig. 1) appear missing or less pronounced in the endpoint mass density change measurement (Fig. 2), best illustrated in FITC-MAA binding to α2-3-linked sialosides (Fig. 2d *vs.* Fig. 1d).

purposes need caution. Though tagged recombinant lectins may better retain binding properties of unlabeled (unconjugated) lectins than amine-based fluorescent labeled lectins as the tag may be constructed far from the glycan-binding pocket of interest, that conclusion still needs confirmation against unlabeled lectins by a label-free method under same assay conditions.

Due to high dissociation rates of many GBP-glycan complexes at room temperatures, endpoints of GBP-glycan binding reactions measured by ex-situ fluorescence-based methods vary with how the reactions are ended and post-reaction processing before fluorescence read-out. As illustrated in MAA and FITC-MAA binding to four α2-3-linked sialosides, different conclusions can be drawn from an endpoint-type assay, depending on when the endpoint is taken. Vigorous washing would have removed most or all lectins captured by the glycans (Fig. 1d and 2d).

Real-time association–dissociation curves, enabled by the label-free detection method, reveal the evidence that more than one GBP-glycan complex form between a lectin and surface-bound glycans. As a result, it can be problematic to describe the steady-state endpoint of a GBP-glycan reaction as being proportional to $[c]/([c] + K_d) = K_a[c]/(K_a[c] + 1)$ with K_a being the sole equilibrium association constant.[14] Such a relationship is routinely used to extract K_a or K_d for protein–glycan interaction in fluorescence-based studies. The potential pitfall is that depending upon the protein concentration [c] and incubation time, the apparent K_d is dominated by different protein–glycan complexes (Fig. 1a and b), rendering the information not a suitable characteristic of the interaction.

Further experimental evidence of multiple presentations of a surface-immobilized glycan target (referred as multiple sites in this work) for a glycan-binding protein

From the association–dissociation curves that we have reported here, one can see clearly that a glycan-binding protein probe forms more than one type of complexes with the "same" immobilized glycan targets, and each complex has characteristic association and dissociation rate constants. The question is

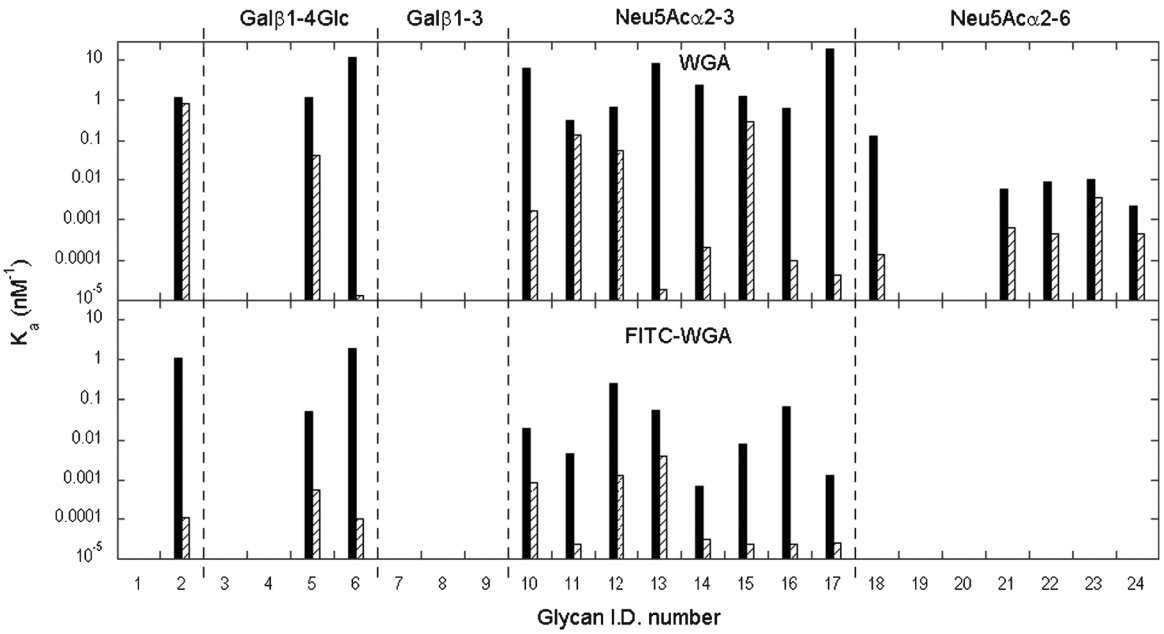

Fig. 3 Equilibrium association constants of WGA (top panel) and FITC-WGA (bottom panel) binding to 24 glycans. For each glycan target, the solid column shows the constant to the one of the two sites with higher affinity, and the shaded column shows the constant to the other site with lower affinity. OS-3 through OS-6 have terminal Galβ1-4. OS-7 through OS-9 have terminal Galβ1-3. OS-10 through OS-17 are α2-3-linked sialosides. OS-18 through OS-24 are α2-6-linked sialosides. Unlike non-labeled WGA, FITC-WGA does not bind to α2-6-linked sialosides.

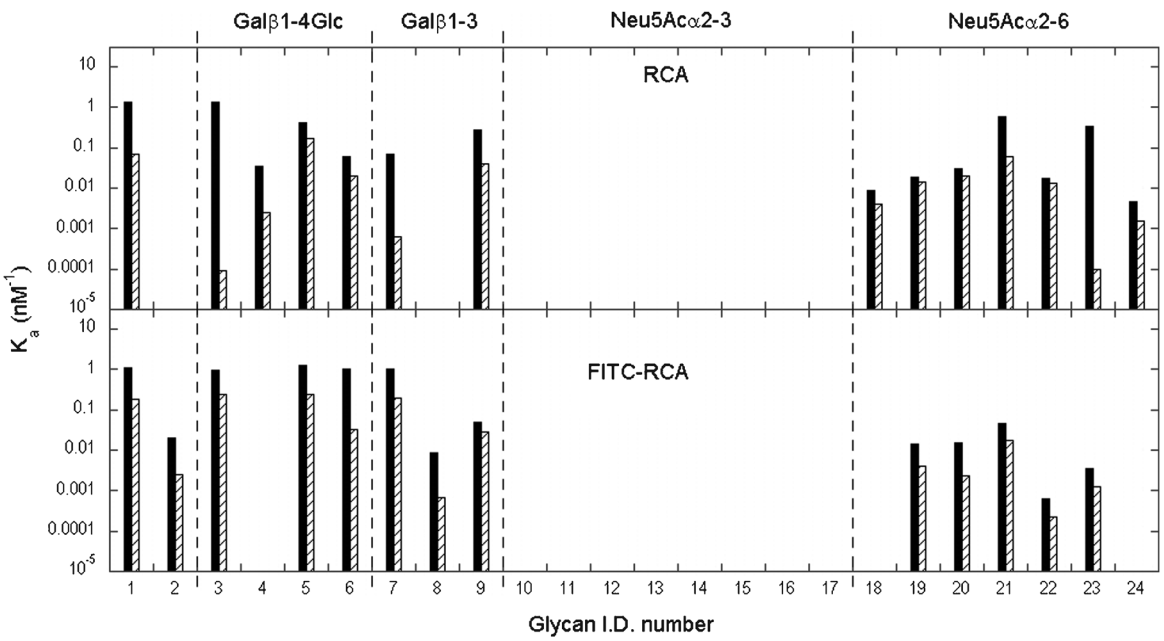

Fig. 4 Equilibrium association constants of RCA (top panel) and FITC-RCA (bottom panel) binding to 24 glycans. FITC labeling significantly changes the affinity profile of RCA, but responding to more detailed glycan structural modifications (*e.g.*, OS-1 *vs.* OS-2, OS-3 *vs.* OS-4, OS-7 *vs.* OS-8, and OS-23 *vs.* OS-24).

whether these different probe-target complexes are formed primarily (a) by the only presentation of the immobilized targets with different binding pockets on the protein probe or (b) by different presentations of the immobilized targets with the same pocket on the probe. In scenarios (a), as long as one of the binding pockets on the protein probe and the immobilized target can form a complex with an equilibrium dissociation constant K_d ($=1/K_a$) comparable to or smaller than the probe concentration [c], the immobilized targets should capture nearly a full monolayer of the protein probes by the end of the association phase. In scenarios (b), on the other hand, even when one presentation of the immobilized targets bind to the pocket on the protein probe with high affinity so that K_d is much less that the probe concentration [c] and thus all the

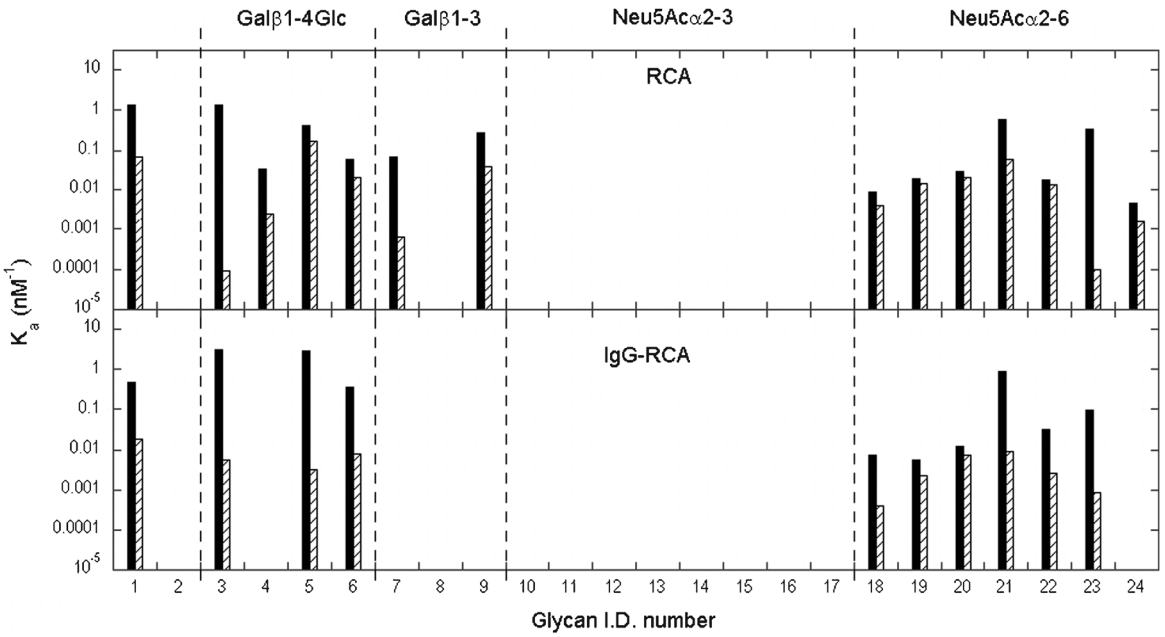

Fig. 5 Equilibrium association constants of RCA (top panel) and goat IgG-RCA (bottom panel) binding to 24 glycans. The precomplex of RCA with goat anti-RCA IgG changes the affinity profile of RCA. Most notably, the affinities to Galβ1-3Glc/GalNAcβ (OS-7 and OS-9) and Neu5Acα2-6Galβ1-3GlcNAcβ (OS-24) are reduced by 5 orders of magnitude to below the detection limit. Yet the binding affinities to similar structures such as Galβ1-4GlcNAcβ and Neu5Acα2-6Galβ1-4GlcNAcβ remain essentially unchanged.

immobilized targets of such presentation capture protein probes successfully, the target surface may not capture a full monolayer of the probes if other presentations of the immobilized targets form complexes with the protein probe with K_d larger than [c]. Based on these considerations, we find that Scenario (b) is supported by the experiment as follows.

The surface mass density of a monolayer of protein probes and the corresponding optical signal can be estimated from the size and molecular weight of the protein. Alternatively, since we record binding curves of a protein probe to many glycan targets simultaneously under the same condition, the optical signal for a monolayer of the captured probes can be estimated as the largest optical signal $\Delta\delta_{max}$ by the end of the association phase across the entire target microarray, regardless the type of the target that produces $\Delta\delta_{max}$. We use $\Delta\delta_{max}$ to examine whether Scenario (a) or (b) is supported. For example Fig. 1c shows the binding curves of unlabeled MAA to 24 glycans from which we identified OS-3, OS-6, and OS-11 through OS-14 as ligands of the proteins (since we use the same scale for all 24 binding curves, the association–dissociation curves to OS-3 are not obvious and yet become clear when we zoom in). As displayed in Fig. S4, the equilibrium dissociation constants K_d of the more stable MAA-glycan complexes (Site 1) for all 6 glycans are below 100 nM (*i.e.*, K_a's are above 0.01 nM^{-1}) which is much smaller than the MAA concentration of [c] = 3 μM. If Scenario (a) dominated, we would expect the optical signals from all 6 targets by the end of association phase to reach values comparable to the maximum value $\Delta\delta_{max}$ in Fig. 1c. But this does not happen. The optical signals for 4 sialosides (OS-11 to OS-14) do reach a comparable level of 8 units corresponding to a surface mass density of 4×10^{-7} g cm^{-2} for the captured MAA. By contrast the optical signals for OS-3 and OS-6 reach much lower levels, indicating that the surface mass density of MAA captured by Galβ1-4Glcβ (OS-3) is only 2.5×10^{-8} g cm^{-2} or 1/16 of those by any one of 4 sialosides. This can only mean that the immobilized OS-3 targets have more than one presentation for MAA. Only the presentations of OS-3 with dissociation constants comparable or less than the MAA concentration will be recorded. The fact that the maximum surface mass density of MAA captured by OS-3 is only 1/16 of MAA captured by OS-12 or OS-13 indicates that the surface number density of those OS-3 with association constants displayed in Fig. S4 is at least 16-fold less than the surface number density of OS-12 and OS-13. As a result, we can conclude that 94% of the immobilized OS-3 has equilibrium association constants above 500 μM (the detection limit of our present real-time binding assay). This finding applies to reactions of all 7 lectins to the 24 glycan targets.

Significance of the minor presentation of glycan targets with large association constants in a binding assay

An *in vitro* binding assay between a protein probe and a ligand (*e.g.*, a glycan in the present study) always involves at least one of the two reactants being situated in a setting different from the *in vivo* environment. As a result the presentations of the protein and/or the ligand are altered from those *in vivo*. Which complex formed by the protein and the ligand most closely represents the *in vivo* one is a difficult question to answer. It is thus important that one acquires information on fractional make-ups of different protein-target complexes and the corresponding association constants. As illustrated in the present study, the simultaneous measurement of binding curves of a protein to multiple immobilized targets enables not only recording binding reactions with a wide range of association

constants but also determining whether the recorded reactions are those between the proteins with major or minor fractions of the immobilized target. We need both types of information to understand the relevance of the affinity profiles obtained by such a binding assay to the corresponding *in vivo* events involving the "same" protein and the "same" ligands.

Materials and methods

Lectins with and without FITC labeling

Ricinus communis Agglutinin (RCA and FITC-RCA with fluorophore-to-protein ratio F/P = 5.4, 120 kDa), *Maackia amurensis* Agglutinin (MAA and FITC-MAA with F/P = 7.1, 130 kDa), *Sambucus nigra* Bark Agglutinin (SNA and FITC-SNA with F/P = 6.9, 150 kDa), and *Erythrina cristagalli* Agglutinin (ECA and FITC-ECA with F/P = 2.5, 54 kDa) were purchased from Vector Laboratories (Burlingame, CA). Wheat Germ Agglutinin (WGA and FITC-WGA with F/P = 1.7, 36 kDa), Peanut Agglutinin (PNA and FITC-PNA with F/P = 2.3, 110 kDa), and *Wisteria floribunda* Agglutinin (WFA and FITC-WFA with F/P = 2.3, 120 kDa) were purchased from EY Laboratories (San Mateo, CA). FITC were conjugated to primary amines (on lysine residues or at the N-terminals) on the lectins to form amide bonds using a proprietary protocol by the vendor. The lectins were diluted with 1× phosphate buffered saline (PBS) to concentrations in the range of μM for real-time binding affinity measurement.

Glycan synthesis and biotinylation

Table 1 lists 24 biotinylated oligosaccharides used in the present study.[21–29] The drawings of these oligosaccharides are available in Supplementary Information. The galactosides,[22,24–26] *N*-acetyl-galactosaminide,[27] α2-3-[24,28]and α2-6-linked[27,29] sialosides with a 3-azidopropyl aglycon were synthesized as reported previously. Biotinylation of these glycans was carried out by reducing the azido group in azidopropyl aglycon to amine and coupled to *N*-hydroxy succinamide (NHS) ester of hexa(ethylene glycol) (HEG)-linked biotin (Biotin-HEG-NHS) as reported previously.[22] All 24 biotinylated oligosaccharides were dissolved in 1× PBS (pH 7.4, 0.22 micron filtered) to the concentration of 50 μM for glycan microarray fabrication.

Glycan microarray on streptavidin-coated glass slide

Using an OmniGrid 100 contact-printing robot (Digilab, Holliston, MA), we printed 4 replicates of each of the 24 carbohydrates on a streptavidin-functionalized slide (ArrayIt, Sunnyvale, CA) to form a 96-spot carbohydrate microarray over an area of 2.6 mm × 3.2 mm. We printed 8 glycan microarrays on one glass slide. The averaged diameter of the printed spots is 130 μm and the center-to-center spot separation is 250 μm. After the excess material was washed off, the printed surface was left with a layer of oligosaccharides enough to capture a monolayer of lectins. Since the size of a streptavidin tetramer on the glass slide is between 5.5 nm and 8 nm, we expect the surface density of streptavidin tetramers to be between 1.6–3.3 × 10^{12} cm^{-2}. Assuming that each tetramer has two biotin-binding pockets available and both pockets successfully capture biotinylated oligosaccharides, we estimate the surface density of the immobilized oligosaccharides to be between 3.3 and 7 × 10^{12} cm^{-2}. This estimate was close to what we observed from the captured lectins by the immobilized oligosaccharides. The printed glass slides were stored at room temperature in a slide box for at least 24 h before further processing for lectin–glycan binding experiments.

Conditions for lectin–glycan binding assays on glycan microarrays

The printed glass slide was assembled with a fluidic system having 8 chambers, each having an active volume of 30 microliters and housing one glycan microarray. The printed surface was washed *in situ* with a flow of 1× PBS. The unprinted part of the surface was blocked with biotin-conjugated bovine serum albumin to prevent non-specific binding of subsequent lectins to streptavidin. For lectin-binding assays, the lectin solution in 1× PBS at a suitable concentration was flown through a chamber at a rate of 2.5 mL/min for a few seconds. The flow rate was then decreased to 0.01 mL/min during the remainder of the association phase of the binding reaction (20 min). At the end of the association phase, 1× PBS was flown through the chamber at a rate of 2.5 mL/min to replace the lectin solution and after a few seconds the flow rate of 1× PBS was reduced to 0.01 mL min^{-1} for the remaining duration of the dissociation phase of the binding reaction (60 min).

Label-free detection of lectin–glycan association–dissociation curves using a real-time ellipsometry-based scanning microscope

Details of the ellipsometry-based scanning microscope, *i.e.*, an oblique-incidence reflectivity difference (OI-RD) scanner, have been described previously.[14,30–32] In essence, the presence of a layer of molecular targets such as glycans on a solid surface such as that of a glass slide and subsequent binding of protein probes to these targets cause changes in the phase and amplitude of an optical beam reflected from the surface. These changes arise from differences in the refractive index of the target-probe layer, the solid support, and the aqueous ambient, and depend on the polarization of the optical beam. The ellipsometry-based scanner measures in real time the differential phase change $\Delta\delta$ between the p-polarized component and the s-polarized component of the optical beam, in much the same way as a surface-plasmon resonance sensor (SPR) measures the resonance angle shift $\Delta\theta_{SPR}$. $\Delta\delta$ is proportional to the surface mass density (gm/cm^2) of immobilized glycan targets and subsequent protein-binding complexes, as does $\Delta\theta_{SPR}$. The ellipsometry-based measurement of a target layer and binding of protein probes to the layer is highly reproducible. The only weakness of such an ellipsometry-based label-free technique is that it is not as sensitive as the fluorescence-based technique. By scanning the focused optical beam across the glycan microarray, we read out the surface mass densities for 96 targets in every 1.8 s during association and dissociation processes of the binding. In the present experiment, one unit of the OI-RD optical signal $\Delta\delta$ corresponds to a surface mass density of 5×10^{-8} g cm^{-2}, assuming that the protein volume mass density is 1.35 g cm^{-3}. For each lectin, the association–dissociation curves (surface mass density *vs.* time) were measured at three lectin concentrations varying over a factor of 4–5. The set of 3

binding curves was globally fit to yield equilibrium dissociation constants $K_d = k_{off}/k_{on}$ or equilibrium association constants $K_a = k_{on}/k_{off}$ (the inverse of K_d).[14] The images of the surface mass density before and after the dissociation phase of the binding were also recorded.

Conclusions

Protein–glycan binding profiles reported in the literatures have been the main source of information for understanding cellular interactions and for mapping the distributions of specific glycans in biological systems. Since the affinity profiles of most glycan-binding proteins (GBPs) have been obtained using fluorescence-based detection, one needs to exert caution before relying on the specifics of these binding affinity profiles for crucial conclusions on cell signaling and cell–cell interaction mechanisms. For example, in tissue staining studies involving fluorescence-labeled GBPs (directly or indirectly through antibodies), dubious binding affinity profiles of the labeled proteins can lead to incorrect mapping of different glycan types in various tissues. The same issue applies to using the reported GBP-glycan affinity profiles to quantify protein or cellular glycosylation patterns without further confirmation.

By the same token, the binding affinity profile of a free-form protein is often used to infer the binding behavior of a virus or a bacterium that expresses such a protein on its surface. Since labeling agents with molecular weights of hundreds of daltons can already alter the binding affinity profile of a protein profoundly, one should expect that the same protein but attached to a viral or bacterial surface can have a significantly altered affinity profile to its ligands. It is thus normal that the binding affinity profile of a free-form protein sometime may not explain the behavior of a bacterial or viral particle that expresses the "same" protein on its surface.

Real-time binding curve measurements over a wide range of protein concentrations are necessary to appropriately determine binding affinity profiles of non-labeled glycan-binding proteins and to quantitatively evaluate the effect of fluorescent labeling agents such as FITC on the affinity profiles as we show in this work.

Acknowledgements

This work was supported by NIH under R01HG003827 (X.D.Z.), R01GM076360-04S1 and R01HD065122 (X.C.).

References

1 *Esssentials of Glycobiolgy*, ed. A. Varki, R. D. Cummings, J. D. Esko, H. H. Freeze, P. Stanley, C. R. Bertozzi, G. W. Hart and M. E. Etzler, Cold Spring Harbor Press, Cold Spring Harbor, NY, 2009.
2 A. E. Smith and A. Helenius, *Science*, 2004, **304**, 237–242.
3 C. R. Bertozzi and L. L. Kiessling, *Science*, 2001, **291**, 2357–2364.
4 J. C. Paulson, O. Blixt and B. E. Collins, *Nat. Chem. Biol.*, 2006, **2**, 238–248.
5 O. Blixt, S. Head, T. Mondala, C. Scanlan, M. E. Huflejt, R. Alvarez, M. C. Bryan, F. Fazio, D. Calarese, J. Stevens, N. Razi, D. J. Stevens, J. J. Skehel, I. van Die, D. R. Burton, I. A. Wilson, R. Cummings, N. Bovin, C. H. Wong and J. C. Paulson, *Proc. Natl. Acad. Sci. U. S. A.*, 2004, **101**, 17033–17038.
6 J. Stevens, O. Blixt, J. C. Paulson and I. A. Wilson, *Nat. Rev. Microbiol.*, 2006, **4**, 857–864.
7 J. Stevens, O. Blixt, L. Glaser, J. K. Taubenberger, P. Palese, J. C. Paulson and I. A. Wilson, *J. Mol. Biol.*, 2006, **355**, 1143–1155.
8 P. H. Liang, C. Y. Wu, W. A. Greenberg and C. H. Wong, *Curr. Opin. Chem. Biol.*, 2008, **12**, 86–92.
9 H. Y. Liao, C. H. Hsu, S. C. Wang, C. H. Liang, H. Y. Yen, C. Y. Su, C. H. Chen, J. T. Jan, C. T. Ren, T. J. Cheng, C. Y. Wu and C. H. Wong, *J. Am. Chem. Soc.*, 2010, **132**, 14849–14856.
10 P. H. Liang, S. K. Wang and C. H. Wong, *J. Am. Chem. Soc.*, 2007, **129**, 11177–11184.
11 T. Feizi and W. Chai, *Nat. Rev. Mol. Cell Biol.*, 2004, **5**, 582–588.
12 A. S. Palma, T. Feizi, Y. Zhang, M. S. Stoll, A. M. Lawson, E. Diaz-Rodriguez, M. A. Campanero-Rhodes, J. Costa, S. Gordon, G. D. Brown and W. Chai, *J. Biol. Chem.*, 2006, **281**, 5771–5779.
13 K. Shinya, M. Ebina, S. Yamada, M. Ono, N. Kasai and Y. Kawaoka, *Nature*, 2006, **440**, 435–436.
14 Y. S. Sun, J. P. Landry, Y. Y. Fei, X. D. Zhu, J. T. Luo, X. B. Wang and K. S. Lam, *Anal. Chem.*, 2009, **81**, 5373–5380.
15 V. P. Bhavanandan and A. W. Katlic, *J. Biol. Chem.*, 1979, **254**, 4000–4008.
16 K. A. Kronis and J. P. Carver, *Biochemistry*, 1982, **21**, 3050–3057.
17 M. Monsigny, A. C. Roche, C. Sene, R. Maget-Dana and F. Delmotte, *Eur. J. Biochem.*, 1980, **104**, 147–153.
18 C. S. Wright, *J. Mol. Biol.*, 1980, **139**, 53–60.
19 J. U. Baenziger and D. Fiete, *J. Biol. Chem.*, 1979, **254**, 9795–9799.
20 H. Debray, D. Decout, G. Strecker, G. Spik and J. Montreuil, *Eur.J. Biochem.*, 1981, **117**, 41–55.
21 X. Chen and A. Varki, *ACS Chem. Biol.*, 2010, **5**, 163–176.
22 H. A. Chokhawala, S. Huang, K. Lau, H. Yu, J. Cheng, V. Thon, N. Hurtado-Ziola, J. A. Guerrero, A. Varki and X. Chen, *ACS Chem. Biol.*, 2008, **3**, 567–576.
23 M. J. Linman, J. D. Taylor, H. Yu, X. Chen and Q. Cheng, *Anal. Chem.*, 2008, **80**, 4007–4013.
24 S. Huang, H. Yu and X. Chen, *Sci. China Chem.*, 2011, **54**, 117–128.
25 H. Yu, V. Thon, K. Lau, L. Cai, Y. Chen, S. Mu, Y. Li, P. G. Wang and X. Chen, *Chem. Commun.*, 2010, **46**, 7507–7509.
26 K. Lau, V. Thon, H. Yu, L. Ding, Y. Chen, M. M. Muthana, D. Wong, R. Huang and X. Chen, *Chem. Commun.*, 2010, **46**, 6066–6068.
27 H. Yu, H. A. Chokhawala, A. Varki and X. Chen, *Org. Biomol. Chem.*, 2007, **5**, 2458–2463.
28 H. Yu, H. Chokhawala, R. Karpel, B. Wu, J. Zhang, Y. Zhang, Q. Jia and X. Chen, *J. Am. Chem. Soc.*, 2005, **127**, 17618–17619.
29 H. Yu, S. Huang, H. Chokhawala, M. Sun, H. Zheng and X. Chen, *Angew. Chem., Int. Ed.*, 2006, **45**, 3938–3944.
30 Y. Y. Fei, J. P. Landry, Y. S. Sun, X. D. Zhu, J. T. Luo, X. B. Wang and K. S. Lam, *Rev. Sci. Instrum.*, 2008, **79**, 013708.
31 J. P. Landry, Y. S. Sun, X. W. Guo and X. D. Zhu, *Appl. Opt.*, 2008, **47**, 3275–3288.
32 Y. Y. Fei, J. P. Landry, Y. S. Sun, X. D. Zhu, J. T. Luo, X. B. Wang, C. Y. Wu and K. S. Lam, *J. Biomed. Opt.*, 2010, **15**, 016018.

